RAPID DIFFUSION OBSERVED IN MICROCRYSTALS BY X-RAY FREE ELECTRON LASER MIX-AND-INJECT SERIAL CRYSTALLOGRAPHY

by

Tek Narsingh Malla

A Thesis Submitted in

Partial Fulfillment of the

Requirements for the Degree of

Master of Science

in Physics

at

The University of Wisconsin-Milwaukee

December 2020

ABSTRACT

RAPID DIFFUSION OBSERVED IN MICROCRYSTALS BY X-RAY FREE ELECTRON LASER MIX-AND-INJECT SERIAL CRYSTALLOGRAPHY

by

Tek Narsingh Malla

The University of Wisconsin-Milwaukee, 2020

Under the Supervision of Professor Marius Schmidt

With time resolved X-ray crystallography (TRX), it is possible to follow reaction progress in real time. The time resolution is achieved by initiating reaction in crystal prior to X-ray exposure, and then collecting diffraction pattern at different time delays. Time resolved serial femtosecond crystallography (TR-SFX) at X-ray free electron lasers (XFELs) allows damage free data collection from microcrystals. Mix-and-inject serial crystallography (MISC) is a type of TR-SFX established at XFELs. In MISC, the reaction in enzymatic crystals is triggered by mixing with a substrate, and the resulting structural changes are probed by XFEL pulses.

Enzymatic reactions are of great interest due to their biological and biomedical significance. Here we employed MISC to study the enzymatic reaction of *Mycobacterium tuberculosis* β-lactamase with ceftriaxone, a third-generation antibiotic. In particular we were interested in the enzyme substrate (ES) complex formation phase that triggers the catalytic reaction. We were able to follow the diffusion of substrate by structural analysis of ES complex at millisecond timescales. We also show the binding of sulbactam, an inhibitor that deactivates β-lactamase. Our results demonstrate

rapid mixing experiments with MISC at XFELs is possible. It allows binding studies of ligands and drugs on other biomedically important enzymes at XFELs.

This thesis is a result of my participation as a member of Prof. Schmidt's research group in an experiment at the European XFEL (EuXFEL). Results of this experiment have been submitted to Nature in November 2020. I have been leading protein purification, crystallization and provided samples to the SPB/SFX instrument at the EuXFEL. In addition, I was participating in data collection, data analysis and data interpretation efforts of which were led by Suraj Pandey at UWM and other members of our international research team.

TABLE OF CONTENTS

LIST OF FIGURES

LIST OF TABLES

1. Introduction

1.1 Overview of X-ray crystallography

All life depends on the specific function of proteins (Alberts, 2002). A protein is a naturally occurring large, complex biopolymer that performs a wide range of functions within organisms. Proteins could be enzymes, antibodies, messengers, structural components, and transport and storage units (Raicu & Popescu, 2008). All proteins are made of several building blocks called amino acids. There are only 20 biogenic amino acids and the organisms use combinations of these 20 amino acids to synthesize any protein they need (Rupp, 2009). These units are covalently bonded to each other forming an unbranched polypeptide chain. One or more of these chains combine and fold into a unique 3-dimensional biologically active structure (Karplus & Weaver, 1976). Proteins shift between several related structures while they operate. Our mission is to understand these functions by obtaining their 3-dimensional molecular structure and observe how the structure changes to perform their function.

As the resolution of optical microscopes is limited to 200 nm, it is impossible to visualize any smaller molecules like protein by traditional means (Hell, 2007). To see the details in atomic resolution, we need comparably short wavelength provided by X-rays. The first protein structure of myoglobin (at 6 Å) was solved in 1950s using X-ray crystallography (Kendrew et al., 1958). Almost 60 years later this method for determination of macromolecular structure is now considered quite mature. Advancement in X-ray sources, and data collection and analysis methods have established X-ray crystallography as the popular choice for structure determination (Garman,

2014). There are several techniques to determine the protein structure but as of today ~89% of the structures have been solved using X-ray methods while other techniques like Electron Microscopy (EM) and Nuclear Magnetic Resonance (NMR) sharing the rest of 11% (Berman et al., 2000). Our lab also specializes in time-resolved X-ray crystallography and henceforth (the contribution of) this technique is discussed in understanding protein structure and dynamics.

1.2 X-ray and protein crystals

As the name implies, X-ray crystallography requires protein crystals to study the molecular structure. To achieve protein crystals, highly purified protein is dissolved in an aqueous precipitating agent to obtain a supersaturated state. The precipitation agent weakens the hydration shell of protein and allows interaction between protein molecules (Bergfors, 1999). Developing protein crystals is a difficult process influenced by many factors, including pH, temperature, ionic strength in the crystallization solution, and even gravity (McPherson & Gavira, 2014). Conformational heterogeneity may also hider successful crystallization so stable, and homogenous protein solutions are required. Even so, determining the optimum crystallization condition is still a trial and error method (Rupp & Wang, 2004). Fortunately, high-throughput robotic methods exist to accelerate and streamline the large number of experiments required to explore the various conditions (High-Throughput Crystallization Screening Center | Hauptman-Woodward Medical Research Institute, *https://hwi.buffalo.edu/high-throughput-crystallization-center/)*.

X-rays are highly energetic and penetrating waves that cannot be focused by lenses. But they scatter weakly when they interact with matter (Thomson, 1896). The scattering is amplified in certain direction when the molecules are arranged in a 3-dimensional lattice like in our (protein) crystals. Essentially, the crystal acts like a 3D diffraction grating causing the incident X-ray beam to diffract only into specific directions (Compton, 1923; Friedrich et al., 1913). Diffraction depends on the size and shape of the repeating unit in the crystal called unit cell and the X-ray wavelength. The intensity of the diffracted patterns however is governed by the arrangement of atoms within the unit cell. These patterns called the Bragg peaks (or Bragg reflections) can be interpreted as the Fourier transform of the object's electron density inside the unit cell (Guinier, 1952). From this electron density, mean positions of atoms can be determined which then gives the structure of the object.

1.3 Sources of X-rays and XFELs

Up to about a decade ago, synchrotrons were the most powerful sources of X-rays and were the driving force of structure biology(Jung et al., 2013; Moffat, 2001). But the pulses produced by them are a few hundred picoseconds long and require exposure times of hundreds of microseconds to seconds in duration to create a suitable diffraction image. So only those intermediates that occur on longer timescales can be investigated (Jung et al., 2013). But important intermediate states are populated on significantly faster timescales, which cannot be observed at -synchrotrons.

Since X-rays are ionizing, they cause significant radiation damage to protein crystals. This effect is amplified if the exposure time is long and crystals are very small. At synchrotrons, this problem has been avoided by avoided keeping the crystals at cryogenic temperature during data collection (Hope, 1988). But cryo-cooling the sample might lead to freezing artifacts. This might interfere with the determination of the native protein structure (Garman & Owen, 2006). Most importantly, protein dynamics is also frozen out, and the protein is not functional.

This changed when hard X-ray Free Electron Laser (XFEL) were introduced in 2009 at Linac Coherent Light Source (LCLS), California. Capable of producing an average flux of 10^{12} photons per pulse which last only tens of femtoseconds, these XFELs are a billion times brighter than the most powerful 3rd generation synchrotrons. At XFELs, X-rays are generated by the principle of self-amplified spontaneous emission (SASE) (Huang & Kim, 2007; Madey, 1971). First, electrons are accelerated to relativistic speed and made to pass through magnetic fields of special array of magnets called undulators. There, they follow curved trajectories emitting X-rays. Electrons further interact with the radiation that they or neighboring electrons emit. Through this interaction all electrons begin emitting coherent radiation. The result is exponential increase of emitted radiation leading to high beam intensities and laser-like properties. Currently there are five XFELs in operation and two more are still under construction.

Even though they only last femtoseconds, the XFEL pulses are so intense that they destroy a protein crystal with a single shot (Lomb et al., 2011). Since diffraction is instantaneous and damage requires some time to evolve, femtosecond X-ray pulses from an XFEL produce essentially damage-free diffraction patterns. This principle of diffraction before destruction was first

demonstrated by computer simulation (Neutze et al., 2000) and later experimentally verified (Chapman et al., 2006, 2011). This also alleviated the need for cryo-cooling and the protein molecules can now be studied at room temperature thus overcoming the shortcomings of synchrotron experiments. Additionally, the brilliant pulses allow crystal sizes to be reduced to the micrometer length scale (microcrystals) and even smaller (Boutet et al., 2012). The smaller crystals are relatively easier to produce and allow homogeneous activation by light or effective diffusion of chemical compounds (described further down).

1.4 Time Resolved-Serial Femtosecond Crystallography (TR-SFX)

In serial crystallography, a large number of small crystals are injected one by one into the X-ray beam in random orientation at room temperature (Chapman et al., 2011). As the crystals are destroyed by the XFEL beam, the serial approach allows crystal to be discarded and immediately replenished by a new one. Since each diffraction image is serially obtained from a fresh crystal, reversible and irreversible processes may be studied in the same fashion. Time resolved (TR) crystallography can be implemented in conjunction by probing the crystals at different time points after reaction initiation (Schmidt, 2015; "Moffat et al," 1992). TR-SX experiments have also been conducted at synchrotron sources (Gati et al., 2014; Roedig et al., 2016). But so far only picosecond resolution has been obtained (Jung et al., 2013; Schotte et al., 2012). The femtosecond pulses of XFEL allowed the temporal resolution to go beyond picosecond regime to femtosecond scales (Pande et al., 2016). In photoactive molecules, a reaction can be initiated by a brief laser flash, called a 'pump' pulse. After an adjustable time-delay, the crystals are illuminated by an X-

ray pulse, called a ‘probe’ pulse, which generates a diffraction pattern. This is called a ‘pump-probe’ experiment (Pande et al., 2016; Pandey, Poudyal, et al., 2020).

Most biologically relevant proteins like enzymes are not photoactive and this method cannot be applied. There have been efforts where the enzymatic reaction was triggered by soaking an inactive, so-called caged substrate into the crystals (Bourgeois & Weik, 2008; Givens et al., 2005). The caged compound is activated by a laser flash and then probed by an X-ray pulse. While this method has potential, only a few time-resolved experiments have so far been reported. A new technique was developed to do time resolved studies in enzymes which is discussed in detail below.

2. Methods and Experiment Design

2.1 Mix and Inject Serial Crystallography (MISC)

Mix and Inject Serial Crystallography is a TR-SX technique in which micron-sized enzyme crystals are mixed with substrate before the mixture is injected into the X-ray interaction region (Kupitz et al., 2017; Schmidt, 2013; Stagno et al., 2017). Figure 2.1 shows the schematic diagram for a general MISC setup. The physics of diffusion is at the heart of MISC. The substrate diffuses into the crystals and initiates a reaction. If reaction initiation through diffusion works, enzyme catalysis can then be observed "on-the-fly", unperturbed, at room temperature and in real time by time-resolved crystallographic methods (Schmidt, 2015; Moffat, 1992).

Diffusion of substrate molecules into protein crystals is governed by Fick's laws of diffusion. Particularly, the second law predicts how diffusion causes the concentration to change with respect to time. It is a partial second order equation of the form

$$\frac{\partial \varphi}{\partial t} = D\nabla^2\varphi \qquad (1)$$

where $\varphi = \varphi(\vec{x}, t)$ is the concentration of substrate that depends both on time and position,

D is the diffusion coefficient,

∇^2 is the Laplacian operator which generalizes the second derivative in 3D space.

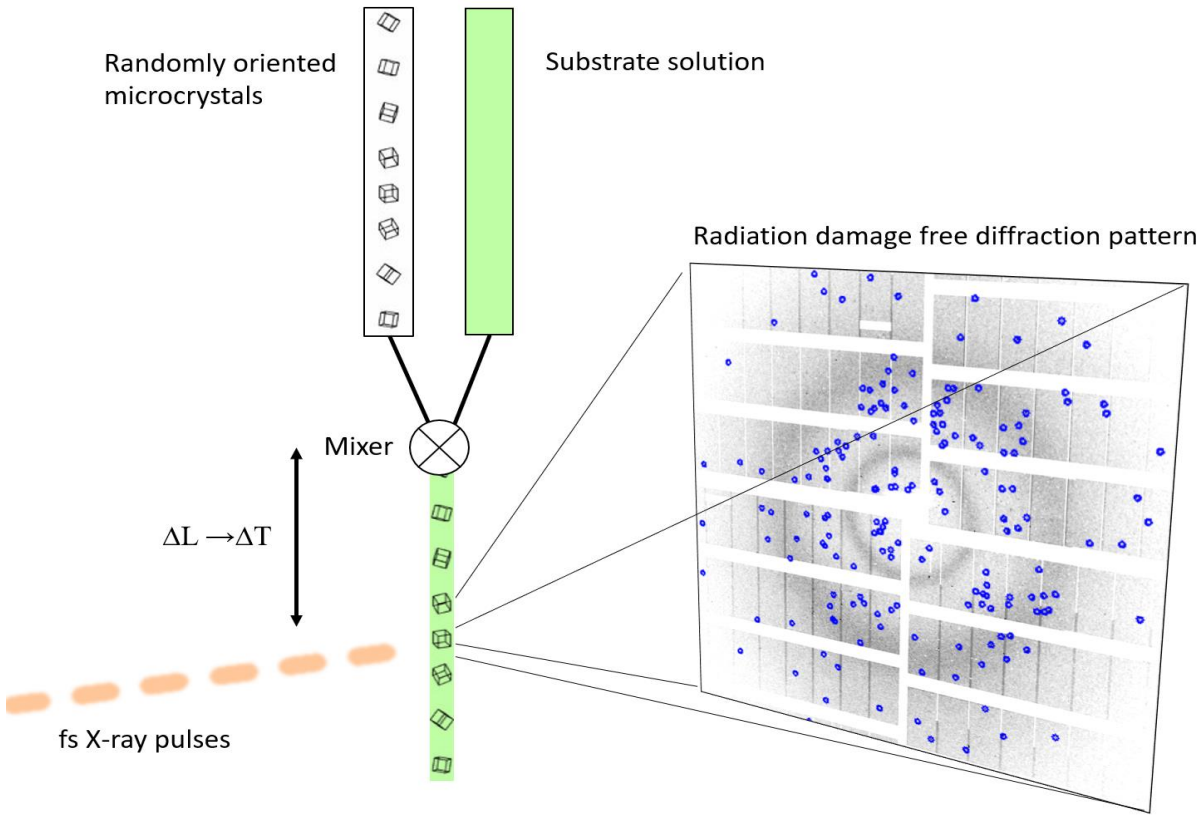

Fig 2.1 *Schematic setup for a mix and inject time-resolved serial crystallographic experiment at XFEL. Crystals and substrate are mixed before being injected into the XFEL beam. The distance from the mixing region to the X-ray interaction region translates to time delay after reaction initiation. Adapted from (Schmidt, 2013)*

With appropriate boundary conditions, this equation can be analytically solved. For example, take a shoe-box-shaped crystal with half edge lengths a, b, and c. The solution is further simplified by assuming the following about the crystals and substrate (Schmidt 2013, 2020): (i) Substrate concentration outside the crystal remains constant throughout the time, (ii) binding of substrate to

the enzyme is neglected, so that the substrate diffuses freely into the crystal, and (iii) mixing of crystal with substrate is instantaneous while the initial concentration inside the crystal is zero (Schmidt, 2013). With these boundary conditions, the solution of equation 1 is given by (Carslaw H. S. & Jaeger J. C., 1959)

$$\varphi(x,y,z,t) = \varphi_0[1 - \frac{64}{\pi^3}\sum_{l=0}^{\infty}\sum_{m=0}^{\infty}\sum_{n=0}^{\infty}\frac{(-1)^{l+m+n}}{(2l+1)(2m+1)(2n+1)} \times cos\frac{(2l+1)\pi x}{2a} cos\frac{(2m+1)\pi y}{2b} cos\frac{(2n+1)\pi z}{2c} \times \exp\left(-\frac{D\pi^2}{4}\left[\frac{(2l+1)^2}{a^2} + \frac{(2m+1)^2}{b^2} + \frac{(2n+1)^2}{c^2}\right].t\right) \quad (2)$$

The concentration of substrate inside the crystal thus depends on the initial outside concentration (φ_0), the position within the crystal, and a time dependent exponential term, called the relaxation rate. The inverse of relaxation rate is defined as the characteristic time τ_c, also called the diffusion time.

$$\tau_c = \frac{4}{D\pi^2\left[\frac{(2l+1)^2}{a^2}+\frac{(2m+1)^2}{b^2}+\frac{(2n+1)^2}{c^2}\right]} \quad (3)$$

This is the time after which the concentration of substrate inside the crystal reaches 69% of the initial outside concentration. It is also obvious that τ_c depends on the square of crystal half lengths. As diffusion into a volume depends on the exposed surface equation (2) is used to calculate the evolution of substrate concentration at the center of crystal and subsequently the time points of TR MISC experiments.

For rapid mixing experiment to work, stoichiometric concentration has to be achieved through diffusion of substrate into crystals. Stoichiometric concentration is the minimum concentration required to establish the full occupancy of substrate in the active site under optimal conditions. A high occupancy results in strong, easily interpretable ligand electron density in the catalytic cleft. Thus, in order to effectively initiate a reaction in crystal by diffusion, (i) the crystals size must be reduced, (ii) the outside substrate concentration φ_0 must be increased, and (iii) the diffusion coefficient must be large (Schmidt, 2020). To address point (i), diffracting crystals as small as possible have to be produced. There has been a lot of studies dedicated to achieving this and are extensively presented by Beale and colleagues (Beale et al., 2019). To reach high substrate concentrations (ii), the ligand needs be highly soluble in the mother liquor that stabilizes the microcrystals. In addition, the substrate can be provided in much larger volumes compared to the crystal volume, so that the depletion of the ligand by diffusion into crystals remains negligible. This may be achieved by mixing the substrate with a much larger flow rate compared to that of the crystals. To promote large diffusion coefficients (iii), solvent channels or pores should be present in the crystal. This is dependent on the crystal morphology. The effect is briefly mentioned later in this thesis and was confirmed by our group's previous experiment (Olmos et al., 2018).

2.2 β-Lactamase (BlaC)

β-lactamases are enzymes produced by bacteria that provide resistance to β-lactam antibiotics. β-lactams are some of the most widely used antibiotics as they are broadly effective against both gram positive and negative bacteria (Lewis, 2013). These include penicillin derivatives (penams), cephalosporins (cephems), monobactams, carbapenems and carbacephems (Murray et al, 2007). β-lactam antibiotics contain a four-atom ring called β-lactam in their molecular structure as shown in the figure 2.2 on the right. Through hydrolysis, the enzyme breaks the β-lactam ring open, deactivating the molecule's antibacterial properties.

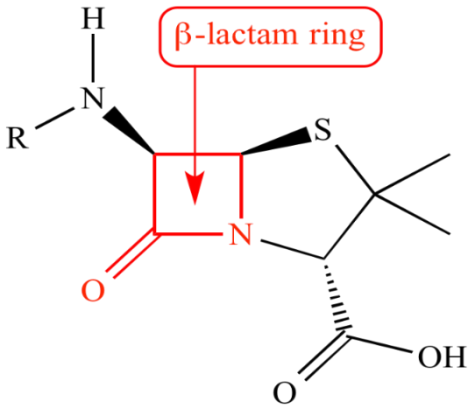

Fig 2.2: *Core structure of penicillin group of antibiotics. All penicillins are β-lactam antibiotics because of the β-lactam ring in their structure.*

Penicillin-binding proteins present in bacterial cell walls catalyze the linkage of N-acetylmuramic acid to N-acetyl-D-glucosamine to form the cell wall (Nelson & Cox, n.d.). β-lactam antibiotics such as penicillins and chemically similar compounds such as the cephalosporins irreversibly inhibit the penicillin-binding protein. Once blocked by these compounds, the enzyme is not able to maintain the integrity of the cell wall and the bacteria perish. Unfortunately, resistance against these. antibiotics was observed shortly after their widespread use. (Fair & Tor, 2014; Walsh, 2000). β-lactamases are found among a large number of possible resistance mechanisms. These enzymes

modify penicillin and related compounds by opening the β-lactam ring. In contrast to the penicillin-binding protein, which is irreversibly and covalently modified by the antibiotic, the β-lactamases bind the antibiotic, catalyze the ring opening, and are finally able to hydrolyze and release the modified product. The free enzyme can now engage in a subsequent cycle of antibiotic modification, eventually rendering the entire amount of administered antibiotics ineffective (Schmidt, 2019).

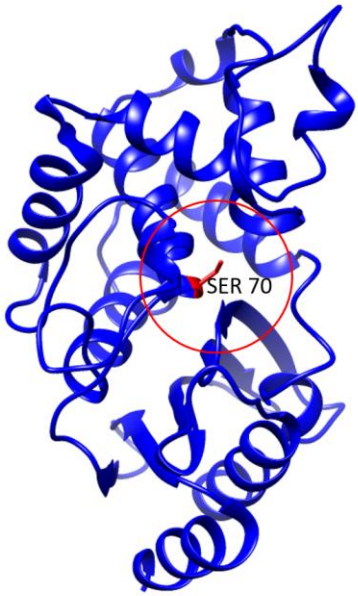

Fig 2.3: *An apo β-lactamase enzyme. Residue serine (Ser 70) at the active site is marked. This along with Ser 128, Thr 237, Lys 73 and Gly 166 forms the catalytic cleft.*

Figure 2.4 shows the catalytic reaction of BlaC with ceftriaxone (CEF), a 3rd generation cephalosporin antibiotic. It has been proposed that the enzyme may use active site interactions to orient the β-lactam carbonyl carbon near the Ser-70 nucleophile (Tremblay, et al., 2010). Nucleophilic attack of Ser-70 results in the opening of the β-lactam ring of CEF (fig 2.4(2)). The antibiotic is then covalently bound to the enzyme forming an acyl intermediate (fig 2.4(3)) (Xu, et al., 2010). A leaving group denoted by R is split off and the antibiotic is inactivated (fig 2.4(2-3)) (Boyd & Lunn, 1979). Finally, the open-ring β-lactam ligand is hydrolyzed and released by the enzyme (fig 2.4(4)).

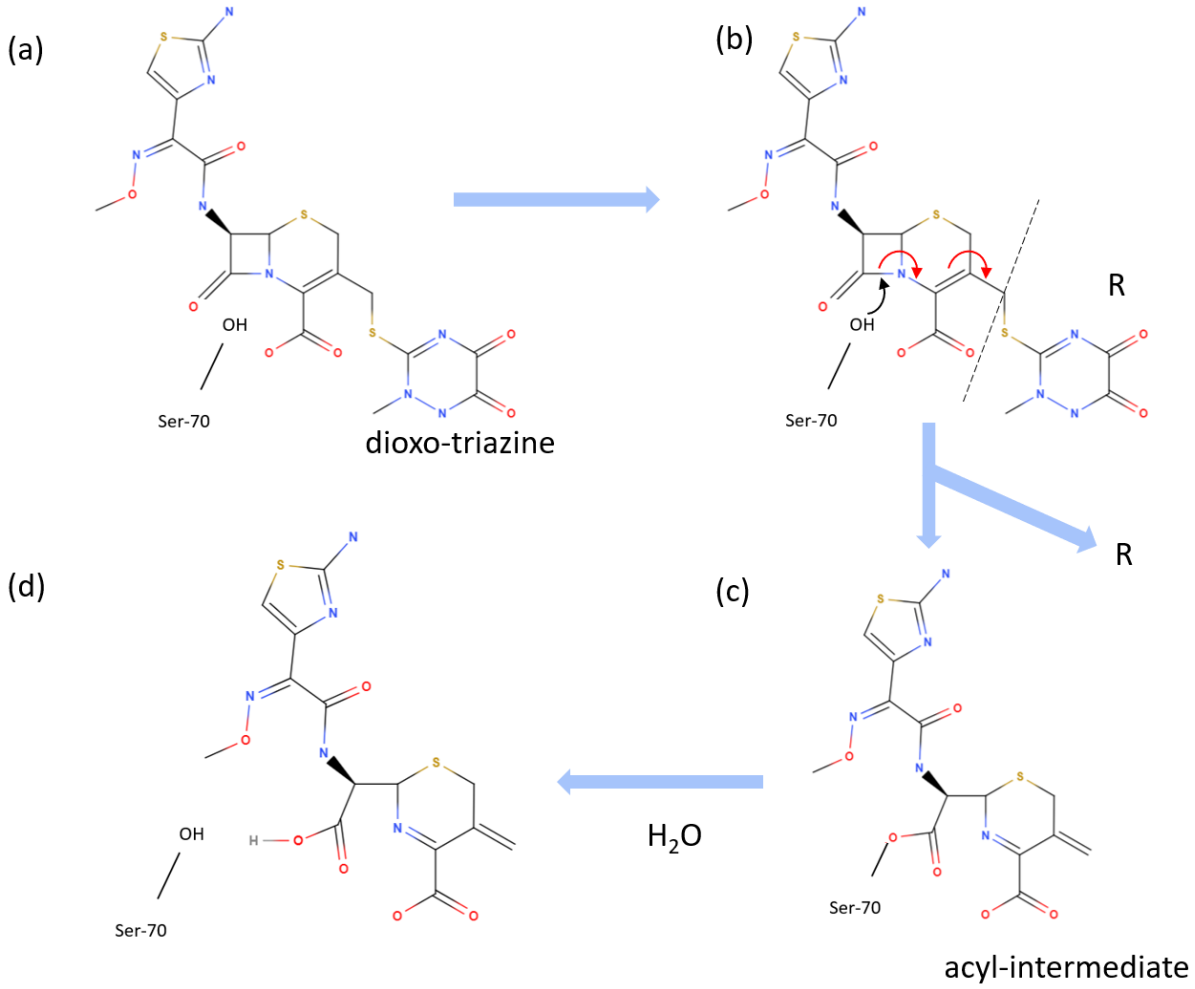

Fig 2.4 *Reaction of β-lactamase with CEF. Only the Ser 70 residue of the enzyme is shown.* ***(1)*** *Formation of enzyme substrate (ES) complex by non-covalent binding of CEF.* ***(2)*** *BlaC catalyzes the opening of the β-lactam ring of CEF by a nucleophilic attack of the active site Ser-70 residue. It causes rearrangement of double bonds (shown by red arrows) which ultimately leads to cleavage of leaving group, R* ***(2-3)****.* ***(3)*** *A reaction intermediate forms where the shortened antibiotics species is covalently bound to the enzyme. This species is called the acyl intermediate.* ***(4)*** *The inactive antibiotic hydrolyzes and leaves the enzyme which is now free to attack another antibiotic molecule. Adapted from (Olmos et al., 2018)*

Here, we have studied *Mycobacterium tuberculosis* (MTB) β-lactamase. MTB causes tuberculosis in humans which causes around a million deaths every year (*https://www.who.int/news-room/fact-sheets/detail/tuberculosis*). The evolution of BlaC has rendered the various classes β-lactam antibiotics ineffective, thereby evading the treatment of tuberculosis (Tremblay, Fan, et al., 2010). Hence, the results of BlaC experiments are biomedically significant. Besides, BlaC forms well-diffracting microcrystals, and β-lactam antibiotics are readily available and very soluble in most cases. This was the prerequisite for MISC experiment. The crystals are so small, diffusion times are fast; much shorter than the time required for one catalytic turnover. BlaC reaction process is simple enough that the enzyme can be used as a model system to establish structure-based enzymology at the XFEL. If the BlaC reaction can be followed, this approach will also work with other important enzymes (Schmidt, 2019, 2020).

2.3 BlaC sample preparation

BlaC was overexpressed and purified as reported by our lab's previous experiments (Kupitz et al., 2017; Olmos et al., 2018). The purified protein was then concentrated to 120mg/ml ~ 150mg/ml and stored at -80 °C. These frozen protein aliquots were transported to European XFEL (EuXFEL) for onsite crystallization right before the experiment. Microcrystals were grown with ammonium phosphate (pH 4.1) as a precipitant using a free interface diffusion method. Purified protein was slowly added dropwise to a vile containing 2.4M ammonium phosphate solution in 1:9 ratio and stirred overnight for 12 hours. The solution was let stand for 2 days. This resulted in shard/(platelet) shaped crystals (fig 2.5). Another crystal form in the shape of needles had also been produced and investigated by our lab previously. In the shards form, the protein forms a large tetramer before conforming to a crystalline structure and displays large solvent channels in all 3 directions (fig 2.6). This allowed us to observe rapid diffusion in crystals. However, in the needle form, individual protein molecules are densely packed in the crystal. This form displays substantially smaller solvent channels. Diffusion of substrate seemed to be slowed down but was not restricted enough to impair effective substrate binding (Olmos et al., 2018).

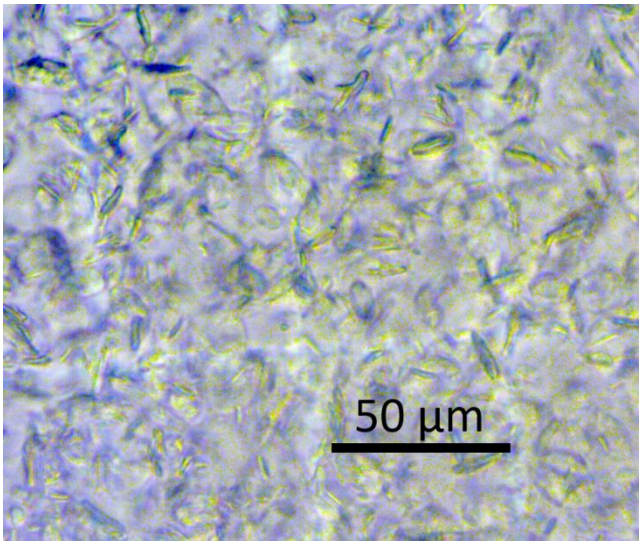

Fig 2.5*: BlaC crystals grown and pictured in the Schmidt Lab, UWM*

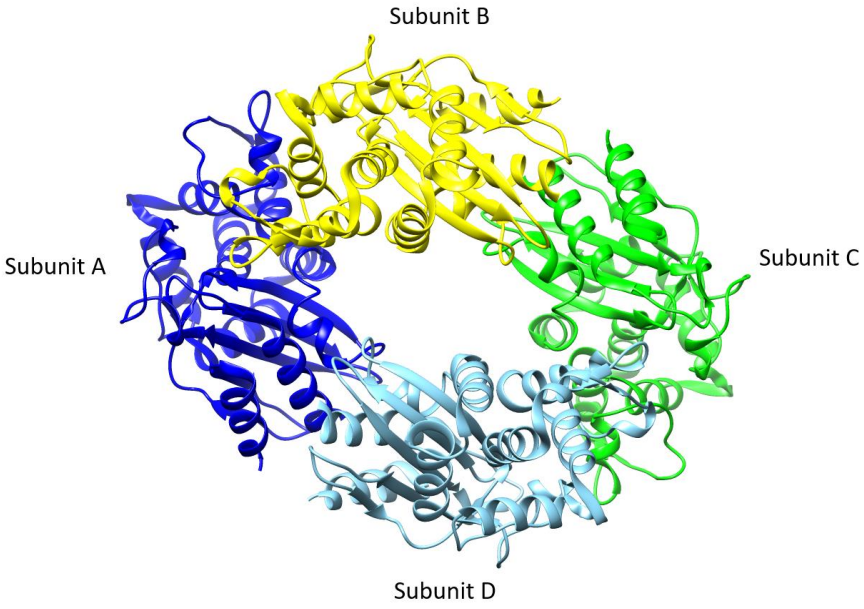

Fig 2.6 Asymmetric subunits of BlaC in shard type crystal

2.4 Data Collection and processing

A MISC experiment with BlaC was conducted at the European XFEL (EuXFEL) in March 2020. Located in Hamburg, Germany, this 3.4 km long facility is the world's largest X-ray laser. It uses super conducting technology to generate very high X-ray pulse rates. The EuXFEL delivers X-rays in pulse trains that repeat 10 times per second . At full specification, each train contains up to 2700 individual X-ray pulses. (Wiedorn et al., 2018).

Data was collected at the SPB/SFX instrument at the EuXFEL (Mancuso et al., 2019). The microcrystal slurry was first filtered through 20 um filter and then through 10 um filter. This resulted in crystals with an approximate size of 10 x 10 x 2 μm^3 which were probed by the XFEL

beam. Each pulse train contained 202 X-ray pulses with 40 fs full width at half maximum (FWHM) pulse duration, and about 1.5 mJ energy per pulse. The pulse repetition rate was 564 kHz, a reduction from the possible 4 MHz to avoid that pristine, upstream jet volumes are affected by previous X-ray pulses (Pandey, Bean, et al., 2020). The X-ray beam size at the jet position was < 5 μm.

Table 2.1 Experimental parameters for mixing injectors (compiled by the Pollack lab, and published in Pandey et al. 2020)

Mixing	**Water**	**SUB 66 ms**	**CEF 5 ms**	**CEF 10 ms**	**CEF 50 ms**
Ligand conc.	na	100 mmol/L	200 mmol/L		
Ligand buffer	na	0.8 mol/L ammoniumphosphate, pH 4.6			
Ligand flow [μL/min]	74.5	54.5	76.7	74.5	71.8
Crystal flow [μl/min]	5.5	11.6	3.3	5.5	8.2
Mixing injector capillary ID [μm]	50	75	50	50	75
Constriction Length [mm]	17.8	36.1	9.3	17.8	36.1
Timing uncertainty [ms]	na	9.3	1.8	3.0	10.4
Time to collect the dataset	50 min	56 min	138 min	250 min	32 min

Mixing was achieved with specialized, optimized mixing injectors, which were adapted to work at the EuXFEL (fig. 2.6). The design of the mixers allowed us to achieve the shortest MISC time points at the time, along with the high speed of the jet that is a requirement for MHz measurements. 200 mmol/L CEF was mixed with the shards and probed at time delays of 5 ms, 10 ms and 50 ms.

Reaction with sulbactam (SUB), a BlaC inhibitor was also probed after 66 ms. The table below shows the different parameters of the injectors utilized to obtain the required timepoints.

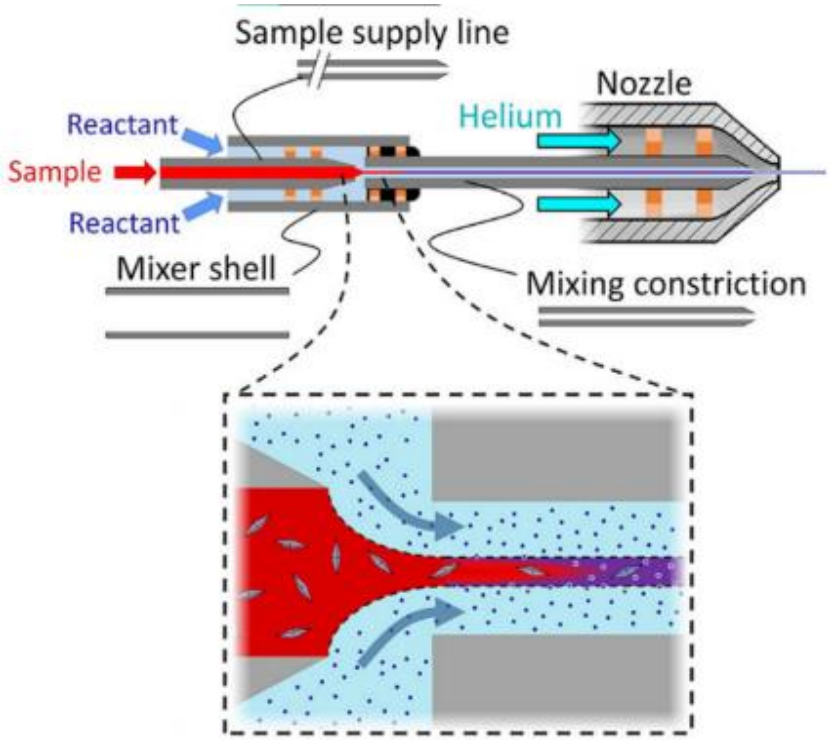

Fig 2.7*: Schematic of optimized injector for MISC used in the experiment. Crystals and reactant flow concentrically down two glass capillary tubes before being combined into a single outlet with a reduced diameter. Cartoon close-up of the focusing region shows diffusion of reactant across the crystal containing jet. Arrows show the direction of flow of various components.(Calvey et al., 2016)*

Diffraction patterns with Bragg reflections were selected by Cheetah (Barty et al., 2014), and indexed, integrated, scaled and merged by CrystFEL(White et al., 2012). Structure factor amplitudes were generated from the intensities using suite of programs from Collaborative

Computational Project Number 4 (CCP4) (Winn et al., 2011). These structure factor amplitudes are then used to calculate difference electron density (DED) maps. If the crystal structure after reaction remained isomorphous, a DED_{iso} map is calculated simply by subtracting unmixed structure facture amplitudes from the mixed structure factor amplitudes. The positive feature of DED_{iso} map represents the new electron density observed in the structure while a negative feature represents the electron density that vanished from the structure. If the structural changes are so large that the unit cell parameters change substantially, a DED_{omit} map is calculated.

At the time of writing of thesis, a manuscript for publication in *Nature* has been submitted based on the findings and the reports of this experiment. I lead the sample preparation part of the experiment. Data were analyzed by Suraj Pandey, a senior graduate student of our team. Occupancy refinement of CEF in BlaC was also explored and executed by Mr. Pandey. My supervisor and PI of the experiment, Prof. Marius Schmidt produced the final figures and interpreted the data. While writing this thesis, I repeated some parts of the data processing and analysis. Results may slightly differ from the manuscript, but the core findings and the main conclusions will remain unchanged.

The table below shows the contribution of key members in parts of the experiment. Appendix A contains the names and affiliation of all the members involved in this experiment.

Table 2.2 Work contribution of key members

Role	Main Contributors	Institution
Protein Purification	Tek Malla: 80%, Suraj Pandey: 15%, a small amount was obtained from the Phillips Lab: Rice University, Houston, TX.	UWM, Rice
Crystallization	Suraj Pandey, Jose Martin-Garcia	UWM, ASU
Mixing Injectors	George Calvey, Andrea M. Katz, Kara A. Zielinski (Pollack Lab).	Cornell University
Data collection	European XFEL staff at the SPB/SFX instrument with Tek Malla, Suraj Pandey, and members of the Fromme lab, ASU, AZ: Faisal H. M. Koua, Jose Martin-Garcia, Jay-How Yang	EuXFEL, UWM, ASU
Data processing	Suraj Pandey with assistance from researchers from the Center for Free Electron Laser Sciences at DESY, Hamburg, Germany (Chapman group).	UWM, CFEL
Data analysis	Suraj Pandey, Marius Schmidt	UWM

Table 2.3. Data Collection Statistics (Obtained from Pandey et al., 2020)

Temperature	293 K		
EXFEL train pulse rate	562 kHz		
	water (reference)	**5 ms CEF**	**10 ms CEF**
Unit Cell a b c in Å, β^{O}	81.0 99.5 112.6, 108.4	80.6 98.8 113.1, 108.6	80.6 98.5 113.5, 108.8
Resolution	2.8 Å	2.4 Å	2.6 Å
Hits	51980	110698	85775
Hit/indexing rate [%]	2.98/61.2	0.65/95.3	1.33/61.0
reflections observed	31,572,191	114,717,921	49,576,617
Unique reflections	41870	65232	51595
Redundancy	754 (236)	1758 (1246)	966.3 (580.4)
Completeness (%)	100(100)	100(100)	100(100)
R-split (%)	20.6 (988)	15.6 (303.7)	17.8 (334)
CC1/2 (%)	96.5 (22.9)	99.2 (26.9)	99.6 (58.4)
	50 ms CEF	**60 ms sulbactam**	**30 ms CEF** (Olmos et al., 2018)
Unit Cell a b c in Å, β^{O}	80.5 98.1 115.4, 110.0	81.0 99.5 112.6, 108.4	78.7 96.8 112.6, 109.7
Resolution	2.6 Å	2.7 Å	2.7 Å
Hits	85914	35886	35,065
Hit/indexing rate [%]	2.26/42.2	0.78/69.7	3.87/69.5
reflections observed	38,055,135	18,745,033	
Unique reflections	50,760	38,338	
Redundancy	749.7 (449.4)	488.9(327.4)	526(142)
Completeness (%)	100(100)	100(100)	100(100)
R-split	20.9 (198.1)	21.4(331.2)	14.2(121.1)
CC1/2	99.5 (58.4)	96.9(21.3)	98.6(34.5)

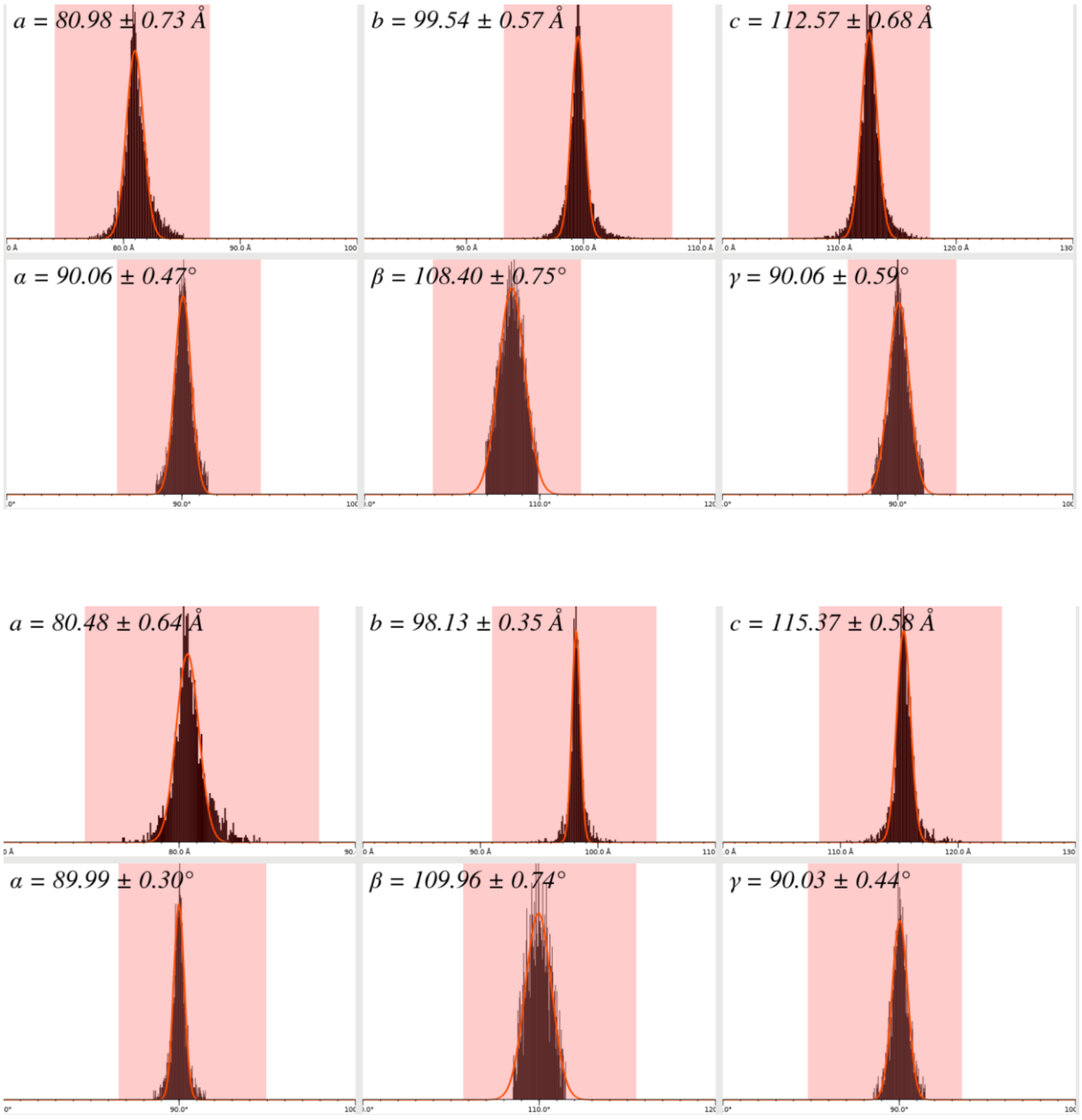

Fig: 2.8 *Unit cell parameters of unmixed BlaC (top) and BlaC mixed with CEF for 50 ms (bottom) calculated by "cell_explorer". "Cell_explorer" is a part of CrystFEL suit of programs that allows to visualize the distributions of unit cell parameters resulting from processing a series of diffraction patterns (Reproduced from Pandey et al., 2020).*

3. Results and discussion

The Apo structure of BlaC and ligand bound structures at different time points after reaction initiation were measured at room temperature. Prior to my involvement our team had already carried out two MISC experiments with BlaC at the Coherent X-ray Imaging (CXI) instrument at the LCLS. The first provided a proof of concept for the feasibility of MISC at XFELs (Kupitz et al., 2017). The second demonstrated that MISC is able to obtain structures of enzymatic reactions in progress(Olmos et al., 2018). Using the cephalosporin antibiotic ceftriaxone (CEF), mixing times as low as 30 ms were achieved. However, at 30ms already full occupancy of the CEF was observed and the substrate binding kinetics remained elusive. We used the rapid repetition rate of EuXFEL pulse to study both diffusion and binding of the large CEF molecule directly on timescales much faster than 30 ms (fig. 1). In addition, we were interested in the reaction of the BlaC with an inhibitor, sulbactam (fig 2.2) on a millisecond time scales.

3.1 Mixing with Ceftriaxone

Three different time delays (5 ms, 10 ms, and 50 ms) were probed for CEF. Because the unit cell parameters changed after mixing (table 1, fig 2.7), DED_{omit} maps were used to determine the structures of the BlaC-CEF complexes. CEF only binds to subunits B and D. Subunits A and C do not show density for CEF even 2 s after mixing (Olmos et al., 2018). Figure 3.1 shows binding

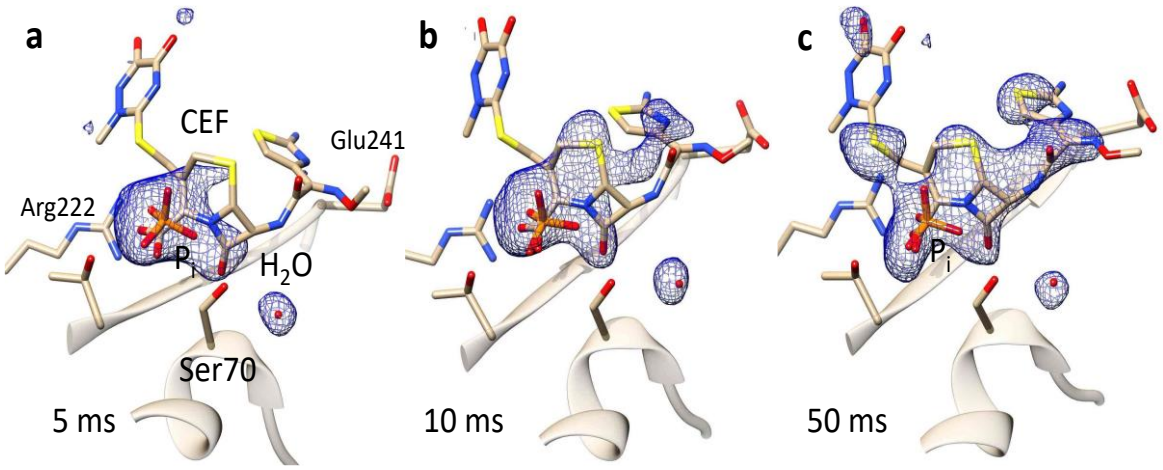

Fig 3.1 *Omit difference electron density in the active center of BlaC of subunit B. (a) 5ms, (b) 10 ms after mixing and (c) 50 ms after mixing. Ser-70, CEF, the phosphate (P_i) and the water molecule are marked in (a). Some nearby amino acids are also displayed in addition. Data analyzed and figure produced by S. Pandey and M. Schmidt (Pandey et al., 2020).*

of ceftriaxone at the binding site of subunit B of BlaC at different time points. Although weak, electron density of CEF at 5 ms shows that the rapid diffusion of substrate into the crystals was successful. The map shows the phosphate molecule on equal par. On the average, every other BlaC molecule binds to either a phosphate or a CEF. This phosphate occupies the same position near the Ser-70 in the unmixed form. The electron density of the phosphate is still visible at 10 ms. Finally, after 50 ms, the phosphate density vanishes. Unit cell parameter changes along with increasing timepoints which correspond to CEF binding and phosphate release (table 1, fig 3.2). We believe that both the size of the ligand as well as the replacement of the strongly negatively charged phosphate contribute to the unit cell changes. In the inactive subunits A and C, two glutamines (Gln-109 and Gln-112) from adjacent subunits extend into the catalytic cleft. This arrangement clashes with accommodation of the large CEF in the binding pocket.

In enzymatic mixing experiments, formation of the enzyme-substrate (ES) complex determines the start of time resolution for the enzymatic cycle. The ES complex formation depends on the substrate concentration, the reaction rate coefficients, the diffusion coefficient and the free enzymes inside the crystals. The substrate is delivered into crystals by diffusion. But MISC does not measure diffusion directly. Instead we observe the increase of occupancy of substrate in crystals to estimate the diffusion of substrate inside crystals. Increased occupancy of substrate is the direct result of ES complex formation. As substrate occupancy increases free enzyme occupancy decreases. Occupancy refinement by Phenix (Liebschner et al., 2019) shows that 50 % of the BlaC active sites B and D are occupied by CEF and 50 % are free of ligand at 5 ms (Pandey et al., 2020). In a previous publication, the k_{on} rate coefficient was estimated to be 3.2 L/mmol s^{-1} while assuming a negligible k_{off} rate coefficient (Olmos et al., 2018). With these parameters known, we can use equation 2 to estimate the diffusion coefficient with which the occupancy of ES complex is 50% at 5ms. The effective diffusion coefficient of 2.0 x 10^{-7} cm^2/s is obtained (Pandey et al., 2020) which is much smaller than the diffusion coefficient in water, 3 x 10^{-6} cm^2/s (Majidi et al., 2011). Our BlaC crystals were of the size10 x 10 x 2 μm^3 in average. In water it would have taken 1.6 ms to reach full occupancy in the same volume. If we can get even smaller crystals, ES formation rate could even be faster due to reduced diffusion time. With sufficiently small microcrystals, though, binding of substrate may become rate limiting instead of diffusion of substrate into crystal. In enzymes with fast turnover rates, the crystal size has to be adjusted to compensate for increased binding rates (Pandey et al., 2020). Hence for an effective mixing experiment, it is equally important to consider the chemical binding kinetics in addition to the diffusion rates.

3.2 Mixing with Sulbactam

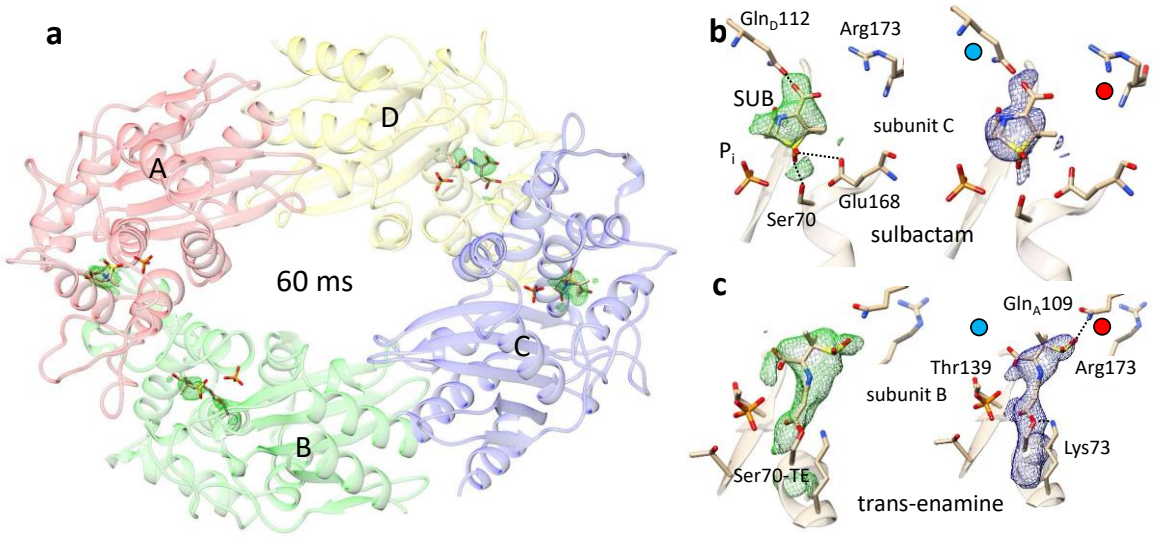

***Figure 3.2**. Sulbactam binding. (a) SUB binds to all four subunits of BlaC. The phosphates in the active sites are not replaced. DED$_{iso}$ map (2 sigma) shown in green. (b) Active site in subunit C with non-covalently bound intact sulbactam, left side: DED$_{iso}$ map, right side: weighted DED map after refinement. (c) Active site in subunit B with trans-enamine bound to Ser-70, left side: DED$_{iso}$ map, right side: weighted DED map after refinement. Red and blue dot show important differences between the subunits. Gln112 from the adjacent subunit is not located close-by, and the Arg173 is extended in subunit B leaving subunit B more accessible to ligands and substrate. (Figure provided by M. Schmidt, Pandey et al., 2020)*

Unlike CEF, SUB electron density was observed in all four subunits in the asymmetric units (fig 3.2 (a)). The phosphate also does not leave the active site. Surprisingly though, the disparity in subunits is also present here. The DED$_{iso}$ map is different for subunits A, C and B, D.

In the “active” subunits B and D, the electron density is elongated such that, it can be interpreted as a sulbactam *trans*-enamine (EN) covalently bound to Ser-70 (fig 3.2 (c)). The reaction pathway of BlaC with SUB has already been reported before. Ser-70 of the BlaC opens the β-lactam ring, the structure rearranges to an imine, which either transforms to a *cis*-enamine, or to a *trans*-enamine covalently bound to Ser-70 (fig 3.3). This irreversible binding inactivates the BlaC (Padayatti et al., 2005). In our results we only see the of trans-EN.

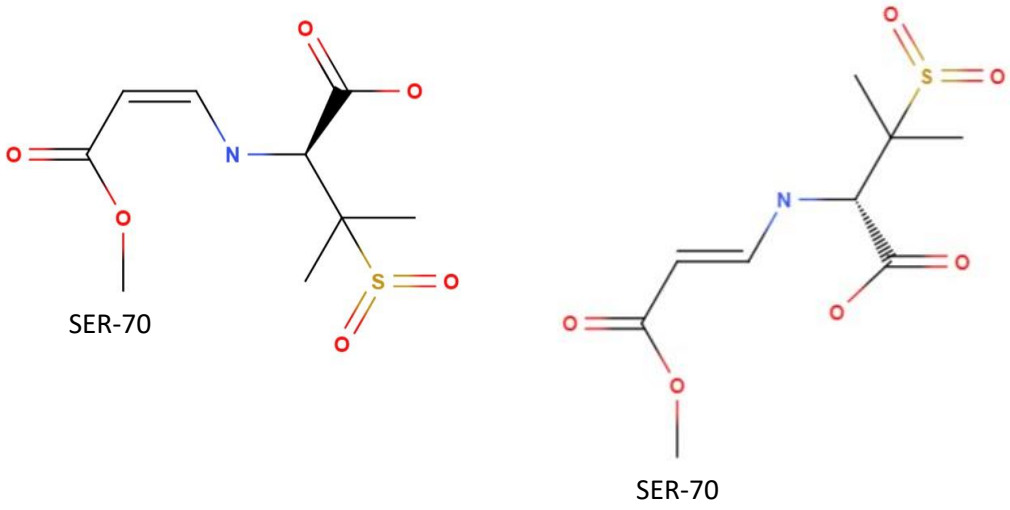

Fig 3.3 *Two possible conformation of sulbactam after binding to BlaC. Cis-enamine (left) and trans-enamine (right). We only observed the presence of trans-enamine.*

In “inactive” subunits A and C, the electron density appears in such a way that an intact SUB can be fitted (fig 3.2(b)). Unlike in B and D, the SUB molecule is not covalently bound to the active site, and is oriented such that the β-lactam ring is pointing away from Ser-70. This could again be due to the interference with glutamine from the adjacent subunits. It is the same glutamine that prevented CEF binding earlier. As the SUB is smaller than CEF, it could enter into the active site

but there is not enough room for it to reorient itself in a correct way for effective binding. This finding shows that the packing of molecules inside a crystal also plays an important role in the binding kinetics.

Because SUB is smaller than CEF, we expect the diffusion time to be shorter. When observed after 60 ms, all the non-covalently bound SUB molecules in subunits B and D have reacted to form the covalently bound trans-EN. The early stages of chemical reaction between Ser-70 and SUB have eluded observation. Shorter time delays are thus necessary to observe this faster kinetics. On the other hand, we can see SUB non-covalently bound to BlaC in subunits A and C, but the reaction has not taken place yet. It is not clear if reaction needs more time to complete or the interference at the catalytic cleft prevents the reaction altogether. In either case experiments exploring longer time delays will clarify the situation. On an additional note: a recent experiment at the LCLS (LU68) that explored SUB binding and reaction to BlaC showed a trans-enamine in the catalytic cleft of the less-active subunit C on longer ms timescales (unpublished, data analysis ongoing). That indicates that eventually all active centers will covalently bind this inhibitor.

4. Conclusion and outlook

In this study we structurally characterized real-time substrate binding in BlaC microcrystals, and also demonstrated direct structural evidence for the mechanism of the BlaC enzymatic activity. This information contributes to our understanding of how antibiotics react and are potentially eliminated on a millisecond time scale. The rapid diffusion observed with CEF shows that the mix-and-inject technique can be used to characterize enzymes with turnover times much faster than the BlaC and perform binding studies of ligands and drug molecules as well as other biomedically important enzymes at XFELs. Since SUB showed promising results and is even smaller than CEF, we plan to push the time resolution of MISC to the limit by using SUB in the future MISC experiments with BlaC.

The direct investigation of the catalytic functions of many biologically and biomedically highly significant enzymes with the mix-and-inject technique is the focus of macromolecular TR-SFX (Schmidt, 2020). Our team has already conducted a structure-based drug screening experiment to find a potential cure against SARS-CoV-2 using the MISC technology at LCLS (PDB entry 7JVZ). High-repetition-rate XFELs such as the EuXFEL has reduced experimental times to minutes (Yefanov et al., 2019; Pandey et al., 2020). With this, highly efficient fragment screening may become available as drug targets can be tested with numerous compounds within a shift (Schmidt, 2020). All these progresses will help establish XFEL as an invaluable tool for structure-based drug design.

5. References

Alberts, B. , J. A. , L. J. , R. M. , R. K. , and W. P. (2002). Molecular biology of the cell. In *Biochemistry and Molecular Biology Education* (4th ed., Issue 4). Garland Science. https://doi.org/10.1002/bmb.2003.494031049999

Barty, A., Kirian, R. A., Maia, F. R. N. C., Hantke, M., Yoon, C. H., White, T. A., & Chapman, H. (2014). Cheetah: Software for high-throughput reduction and analysis of serial femtosecond X-ray diffraction data. *Journal of Applied Crystallography*, *47*(3), 1118–1131. https://doi.org/10.1107/S1600576714007626

Beale, J. H., Bolton, R., Marshall, S. A., Beale, E. v., Carr, S. B., Ebrahim, A., Moreno-Chicano, T., Hough, M. A., Worrall, J. A. R., Tews, I., & Owen, R. L. (2019). Successful sample preparation for serial crystallography experiments. *Journal of Applied Crystallography*, *52*(6), 1385–1396. https://doi.org/10.1107/S1600576719013517

Bergfors, T. M. (1999). *Protein crystallization : techniques, strategies, and tips : a laboratory manual*. https://ci.nii.ac.jp/ncid/BA41285506

Berman, H. M., Westbrook, J., Feng, Z., Gilliland, G., Bhat, T. N., Weissig, H., Shindyalov, I. N., & Bourne, P. E. (2000). The Protein Data Bank. In *Nucleic Acids Research* (Vol. 28, Issue 1, pp. 235–242). Oxford University Press. https://doi.org/10.1093/nar/28.1.235

Bourgeois, D., & Weik, M. (2008). Kinetic Protein Crystallography using Caged Compounds. In *Protein Science Encyclopedia* (pp. 410–434). Wiley-VCH Verlag GmbH & Co. KGaA. https://doi.org/10.1002/9783527610754.fa19

Boutet, S., Lomb, L., Williams, G. J., Barends, T. R. M., Aquila, A., Doak, R. B., Weierstall, U., DePonte, D. P., Steinbrener, J., Shoeman, R. L., Messerschmidt, M., Barty, A., White, T. A., Kassemeyer, S., Kirian, R. A., Seibert, M. M., Montanez, P. A., Kenney, C., Herbst, R., … Schlichting, I. (2012). High-Resolution Protein Structure Determination by Serial Femtosecond Crystallography. *Science*, *337*(6092), 362–364. https://doi.org/10.1126/science.1217737

Boyd, D. B., & Lunn, W. H. W. (1979). Electronic Structures of Cephalosporins and Penicillins. 9. Departure of a Leaving Group in Cephalosporins. *Journal of Medicinal Chemistry*, *22*(7), 778–784. https://doi.org/10.1021/jm00193a006

Calvey, G. D., Katz, A. M., Schaffer, C. B., & Pollack, L. (2016). Mixing injector enables time-resolved crystallography with high hit rate at X-ray free electron lasers. *Structural Dynamics*, *3*(5). https://doi.org/10.1063/1.4961971

Carslaw H. S., & Jaeger J. C. (1959). *Conduction of Heat in Solids* (2nd ed.). Oxford University Press, USA.

Chapman, H. N., Barty, A., Bogan, M. J., Boutet, S., Frank, M., Hau-Riege, S. P., Marchesini, S., Woods, B. W., Bajt, S., Benner, W. H., London, R. A., Plönjes, E., Kuhlmann, M., Treusch, R., Düsterer, S., Tschentscher, T., Schneider, J. R., Spiller, E., Möller, T., … Hajdu, J. (2006). Femtosecond diffractive imaging with a soft-X-ray free-electron laser. *Nature Physics*, *2*(12), 839–843. https://doi.org/10.1038/nphys461

Chapman, H. N., Fromme, P., Barty, A., White, T. A., Kirian, R. A., Aquila, A., Hunter, M. S., Schulz, J., Deponte, D. P., Weierstall, U., Doak, R. B., Maia, F. R. N. C., Martin, A. v., Schlichting, I., Lomb, L., Coppola, N., Shoeman, R. L., Epp, S. W., Hartmann, R., … Spence, J. C. H. (2011). Femtosecond X-ray protein nanocrystallography. *Nature*, *470*(7332), 73–78. https://doi.org/10.1038/nature09750

Compton, A. H. (1923). A Quantum Theory of the Scattering of X-rays by Light Elements. *Physical Review*, *21*(5), 483–502. https://doi.org/10.1103/PhysRev.21.483

Fair, R. J., & Tor, Y. (2014). Antibiotics and Bacterial Resistance in the 21st Century. *Perspectives in Medicinal Chemistry*, *6*(6), PMC.S14459. https://doi.org/10.4137/PMC.S14459

Friedrich, W., Knipping, P., & Laue, M. (1913). Interferenzerscheinungen bei Röntgenstrahlen. *Annalen Der Physik*, *346*(10), 971–988. https://doi.org/10.1002/andp.19133461004

Garman, E. F. (2014). Developments in X-ray crystallographic structure determination of biological macromolecules. In *Science* (Vol. 343, Issue 6175, pp. 1102–1108). American Association for the Advancement of Science. https://doi.org/10.1126/science.1247829

Garman, E. F., & Owen, R. L. (2006). Cryocooling and radiation damage in macromolecular crystallography. *Acta Crystallographica Section D: Biological Crystallography*, *62*(1), 32–47. https://doi.org/10.1107/S0907444905034207

Gati, C., Bourenkov, G., Klinge, M., Rehders, D., Stellato, F., Oberthür, D., Yefanov, O., Sommer, B. P., Mogk, S., Duszenko, M., Betzel, C., Schneider, T. R., Chapman, H. N., & Redecke, L. (2014). Serial crystallography on in vivo grown microcrystals using synchrotron radiation. *IUCrJ*, *1*(2), 87–94. https://doi.org/10.1107/S2052252513033939

Givens, R., Kotala, M. B., & Lee, J.-I. (2005). Mechanistic Overview of Phototriggers and Cage Release. In *Dynamic Studies in Biology* (pp. 95–129). Wiley-VCH Verlag GmbH & Co. KGaA. https://doi.org/10.1002/3527605592.ch2

Guinier, A. (n.d.). *X-Ray Crystallographic Technology* |. Retrieved November 1, 2020, from https://el.b-ok.org/book/568644/b96f34

Hell, S. W. (2007). Far-field optical nanoscopy. In *Science* (Vol. 316, Issue 5828, pp. 1153–1158). American Association for the Advancement of Science. https://doi.org/10.1126/science.1137395

High-Throughput Crystallization Screening Center | Hauptman-Woodward Medical Research Institute. (n.d.). Retrieved November 1, 2020, from https://hwi.buffalo.edu/high-throughput-crystallization-center/

Hope, H. (1988). Cryocrystallography of biological macromolecules: a generally applicable method. *Acta Crystallographica Section B*, *44*(1), 22–26. https://doi.org/10.1107/S0108768187008632

Huang, Z., & Kim, K. J. (2007). Review of x-ray free-electron laser theory. In *Physical Review Special Topics - Accelerators and Beams* (Vol. 10, Issue 3, p. 034801). American Physical Society. https://doi.org/10.1103/PhysRevSTAB.10.034801

Jung, Y. O., Lee, J. H., Kim, J., Schmidt, M., Moffat, K., Šrajer, V., & Ihee, H. (2013). Volume-conserving trans-cis isomerization pathways in photoactive yellow protein visualized by picosecond X-ray crystallography. *Nature Chemistry*, *5*(3), 212–220. https://doi.org/10.1038/nchem.1565

Karplus, M., & Weaver, D. L. (1976). Protein-folding dynamics. *Nature*, *260*(5550), 404–406. https://doi.org/10.1038/260404a0

Kendrew, J. C., Bodo, G., Dintzis, H. M., Parrish, R. G., Wyckoff, H., & Phillips, D. C. (1958). A three-dimensional model of the myoglobin molecule obtained by x-ray analysis. *Nature*, *181*(4610), 662–666. https://doi.org/10.1038/181662a0

Kupitz, C., Olmos, J. L., Holl, M., Tremblay, L., Pande, K., Pandey, S., Oberthür, D., Hunter, M., Liang, M., Aquila, A., Tenboer, J., Calvey, G., Katz, A., Chen, Y., Wiedorn, M. O., Knoska, J., Meents, A., Majriani, V., Norwood, T., … Schmidt, M. (2017). Structural enzymology using X-ray free electron lasers. *Structural Dynamics*, *4*(4), 044003. https://doi.org/10.1063/1.4972069

Liebschner, D., Afonine, P. v., Baker, M. L., Bunkoczi, G., Chen, V. B., Croll, T. I., Hintze, B., Hung, L. W., Jain, S., McCoy, A. J., Moriarty, N. W., Oeffner, R. D., Poon, B. K., Prisant, M. G., Read, R. J., Richardson, J. S., Richardson, D. C., Sammito, M. D., Sobolev, O. v., … Adams, P. D. (2019). Macromolecular structure determination using X-rays, neutrons and electrons: Recent developments in Phenix. *Acta Crystallographica Section D: Structural Biology*, *75*(10), 861–877. https://doi.org/10.1107/S2059798319011471

Lomb, L., Barends, T. R. M., Kassemeyer, S., Aquila, A., Epp, S. W., Erk, B., Foucar, L., Hartmann, R., Rudek, B., Rolles, D., Rudenko, A., Shoeman, R. L., Andreasson, J., Bajt, S., Barthelmess, M., Barty, A., Bogan, M. J., Bostedt, C., Bozek, J. D., … Schlichting, I. (2011). Radiation damage in protein serial femtosecond crystallography using an x-ray free-electron laser. *Physical Review B - Condensed Matter and Materials Physics*, *84*(21), 214111. https://doi.org/10.1103/PhysRevB.84.214111

Madey, J. M. J. (1971). Stimulated emission of bremsstrahlung in a periodic magnetic field. *Journal of Applied Physics*, *42*(5), 1906–1913. https://doi.org/10.1063/1.1660466

Majidi, M. R., Asadpour-Zeynali, K., & Hafezi, B. (2011). Electrocatalytic oxidation and determination of ceftriaxone sodium antibiotic in pharmaceutical samples on a copper hexacyanoferrate nanostructure. *Analytical Methods*, *3*(3), 646–652. https://doi.org/10.1039/c0ay00582g

Mancuso, A. P., Aquila, A., Batchelor, L., Bean, R. J., Bielecki, J., Borchers, G., Doerner, K., Giewekemeyer, K., Graceffa, R., Kelsey, O. D., Kim, Y., Kirkwood, H. J., Legrand, A., Letrun, R., Manning, B., Morillo, L. L., Messerschmidt, M., Mills, G., Raabe, S., … Tschentscher, T. (2019). The single particles, clusters and biomolecules and serial femtosecond crystallography instrument of the european XFEL: Initial installation. *Journal of Synchrotron Radiation*, *26*(3), 660–676. https://doi.org/10.1107/S1600577519003308

McPherson, A., & Gavira, J. A. (2014). Introduction to protein crystallization. In *Acta Crystallographica Section F:Structural Biology Communications* (Vol. 70, Issue 1, pp. 2–20). International Union of Crystallography. https://doi.org/10.1107/S2053230X13033141

Moffat, K. (2001). Time-resolved biochemical crystallography: A mechanistic perspective. *Chemical Reviews*, *101*(6), 1569–1581. https://doi.org/10.1021/cr990039q

Nelson, D. L., & Cox, M. M. (n.d.). *Lehninger Principles of Biochemistry* (7th ed.). W. H. Freeman.

Neutzo, R., Wouts, R., van der Spoel, D., Weckert, E., & Hajdu, J. (2000). Potential for biomolecular imaging with femtosecond X-ray pulses. In *Nature* (Vol. 406, Issue 6797, pp. 752–757). Macmillan Magazines Ltd. https://doi.org/10.1038/35021099

Olmos, J. L., Pandey, S., Martin-Garcia, J. M., Calvey, G., Katz, A., Knoska, J., Kupitz, C., Hunter, M. S., Liang, M., Oberthuer, D., Yefanov, O., Wiedorn, M., Heyman, M., Holl, M., Pande, K., Barty, A., Miller, M. D., Stern, S., Roy-Chowdhury, S., … Schmidt, M. (2018). Enzyme intermediates captured "on the fly" by mix-and-inject serial crystallography. *BMC Biology*, *16*(1), 59. https://doi.org/10.1186/s12915-018-0524-5

Overview. (n.d.). Retrieved November 10, 2020, from https://www.xfel.eu/facility/overview/index_eng.html

Padayatti, P. S., Helfand, M. S., Totir, M. A., Carey, M. P., Carey, P. R., Bonomo, R. A., & van den Akker, F. (2005). *High Resolution Crystal Structures of the trans-Enamine Intermediates Formed by Sulbactam and Clavulanic Acid and E166A SHV-1-Lactamase **. https://doi.org/10.1074/jbc.M505333200

Pande, K., Hutchison, C. D. M., Groenhof, G., Aquila, A., Robinson, J. S., Tenboer, J., Basu, S., Boutet, S., DePonte, D. P., Liang, M., White, T. A., Zatsepin, N. A., Yefanov, O., Morozov, D., Oberthuer, D., Gati, C., Subramanian, G., James, D., Zhao, Y., … Schmidt, M. (2016). Femtosecond structural dynamics drives the trans/cis isomerization in photoactive yellow protein. *Science*, *352*(6286), 725–729. https://doi.org/10.1126/science.aad5081

Pandey, S., Bean, R., Sato, T., Poudyal, I., Bielecki, J., Cruz Villarreal, J., Yefanov, O., Mariani, V., White, T. A., Kupitz, C., Hunter, M., Abdellatif, M. H., Bajt, S., Bondar, V., Echelmeier, A., Doppler, D., Emons, M., Frank, M., Fromme, R., … Schmidt, M. (2020). Time-resolved serial femtosecond crystallography at the European XFEL. *Nature Methods*, *17*(1), 73–78. https://doi.org/10.1038/s41592-019-0628-z

Pandey, S., Poudyal, I., & Malla, T. N. (2020). Pump-Probe Time-Resolved Serial Femtosecond Crystallography at X-Ray Free Electron Lasers. *Crystals*, *10*(7), 628. https://doi.org/10.3390/cryst10070628

Patrick R. Murray, E. J. B. J. H. J. M. L. L. and M. A. P. W. (2007). Manual of Clinical Microbiology. In *Clinical Infectious Diseases* (9th ed., Issue 1). ASM press. https://doi.org/10.1086/524076

Raicu, V., & Popescu, A. (2008). Integrated molecular and cellular biophysics. In *Integrated Molecular and Cellular Biophysics*. Springer Netherlands. https://doi.org/10.1007/978-1-4020-8268-9

Roedig, P., Duman, R., Sanchez-Weatherby, J., Vartiainen, I., Burkhardt, A., Warmer, M., David, C., Wagner, A., & Meents, A. (2016). Room-temperature macromolecular crystallography using a micro-patterned silicon chip with minimal background scattering. *Journal of Applied Crystallography*, *49*(3), 968–975. https://doi.org/10.1107/S1600576716006348

Rupp, B. (2009). *Biomolecular Crystallography: Principles, Practice, and Application to Structural Biology* (1st ed.). Garland Science. https://www.amazon.com/Biomolecular-Crystallography-Principles-Application-Structural/dp/0815340818

Rupp, B., & Wang, J. (2004). Predictive models for protein crystallization. *Methods*, *34*(3), 390–407. https://doi.org/10.1016/j.ymeth.2004.03.031

Schmidt, M. (2008). *Structure Based Kinetics by Time-Resolved X-ray Crystallography* (pp. 201–241). Springer, Berlin, Heidelberg. https://doi.org/10.1007/978-3-540-73566-3_9

Schmidt, Marius. (2013). Mix and inject: Reaction initiation by diffusion for time-resolved macromolecular crystallography. *Advances in Condensed Matter Physics*, *2013*. https://doi.org/10.1155/2013/167276

Schmidt, Marius. (2015). Time-Resolved Crystallography at X-ray Free Electron Lasers and Synchrotron Light Sources. In *Synchrotron Radiation News* (Vol. 28, Issue 6, pp. 25–30). Taylor and Francis Ltd. https://doi.org/10.1080/08940886.2015.1101324

Schmidt, Marius. (2019). Time-Resolved Macromolecular Crystallography at Pulsed X-ray Sources. *International Journal of Molecular Sciences*, *20*(6), 1401. https://doi.org/10.3390/ijms20061401

Schmidt, Marius. (2020). Reaction Initiation in Enzyme Crystals by Diffusion of Substrate. *Crystals*, *10*(2), 116. https://doi.org/10.3390/cryst10020116

Schotte, F., Cho, H. S., Kaila, V. R. I., Kamikubo, H., Dashdorj, N., Henry, E. R., Graber, T. J., Henning, R., Wulff, M., Hummer, G., Kataoka, M., & Anfinrud, P. A. (2012). Watching a signaling protein function in real time via 100-ps time-resolved Laue crystallography. *Proceedings of the National Academy of Sciences of the United States of America*, *109*(47), 19256–19261. https://doi.org/10.1073/pnas.1210938109

Stagno, J. R., Liu, Y., Bhandari, Y. R., Conrad, C. E., Panja, S., Swain, M., Fan, L., Nelson, G., Li, C., Wendel, D. R., White, T. A., Coe, J. D., Wiedorn, M. O., Knoska, J., Oberthuer, D., Tuckey, R. A., Yu, P., Dyba, M., Tarasov, S. G., … Wang, Y. X. (2017). Structures of riboswitch RNA reaction states by mix-and-inject XFEL serial crystallography. *Nature*, *541*(7636), 242–246. https://doi.org/10.1038/nature20599

Thomson, J. J. (1896). The Röntgen rays. *Nature*, *53*(1382), 581–583. https://doi.org/10.1038/053581e0

Time-resolved crystallography: principles, problems and practice. (1992). *Philosophical Transactions of the Royal Society of London. Series A: Physical and Engineering Sciences*, *340*(1657), 175–190. https://doi.org/10.1098/rsta.1992.0059

Tremblay, L. W., Fan, F., & Blanchard, J. S. (2010). Biochemical and structural characterization of mycobacterium tuberculosis β-lactamase with the carbapenems ertapenem and doripenem. *Biochemistry*, *49*(17), 3766–3773. https://doi.org/10.1021/bi100232q

Tremblay, L. W., Xu, H., & Blanchard, J. S. (2010). Structures of the Michaelis complex (1.2 Å) and the covalent acyl intermediate (2.0 Å) of cefamandole bound in the active sites of the mycobacterium tuberculosis β-lactamase K73A and E166A mutants. *Biochemistry*, *49*(45), 9685–9687. https://doi.org/10.1021/bi1015088

Tuberculosis. (n.d.). Retrieved November 8, 2020, from https://www.who.int/news-room/fact-sheets/detail/tuberculosis

Walsh, C. (2000). Molecular mechanisms that confer antibacterial drug resistance. In *Nature* (Vol. 406, Issue 6797, pp. 775–781). Nature Publishing Group. https://doi.org/10.1038/35021219

White, T. A., Kirian, R. A., Martin, A. v., Aquila, A., Nass, K., Barty, A., & Chapman, H. N. (2012). CrystFEL: A software suite for snapshot serial crystallography. *Journal of Applied Crystallography*, *45*(2), 335–341. https://doi.org/10.1107/S0021889812002312

Wiedorn, M. O., Oberthür, D., Bean, R., Schubert, R., Werner, N., Abbey, B., Aepfelbacher, M., Adriano, L., Allahgholi, A., Al-Qudami, N., Andreasson, J., Aplin, S., Awel, S., Ayyer, K., Bajt, S., Barák, I., Bari, S., Bielecki, J., Botha, S., … Barty, A. (2018). Megahertz serial crystallography. *Nature Communications*, *9*(1). https://doi.org/10.1038/s41467-018-06156-7

Winn, M. D., Ballard, C. C., Cowtan, K. D., Dodson, E. J., Emsley, P., Evans, P. R., Keegan, R. M., Krissinel, E. B., Leslie, A. G. W., McCoy, A., McNicholas, S. J., Murshudov, G. N., Pannu, N. S., Potterton, E. A., Powell, H. R., Read, R. J., Vagin, A., & Wilson, K. S. (2011). Overview of the CCP4 suite and current developments. In *Acta Crystallographica*

Section D: Biological Crystallography (Vol. 67, Issue 4, pp. 235–242). Acta Crystallogr D Biol Crystallogr. https://doi.org/10.1107/S0907444910045749

Yefanov, O., Oberthür, D., Bean, R., Wiedorn, M. O., Knoska, J., Pena, G., Awel, S., Gumprecht, L., Domaracky, M., Sarrou, I., Xavier, P. L., Metz, M., Bajt, S., Mariani, V., Gevorkov, Y., White, T. A., Tolstikova, A., Villanueva-Perez, P., Seuring, C., … Barty, A. (2019). Evaluation of serial crystallographic structure determination within megahertz pulse trains. *Structural Dynamics*, *6*(6). https://doi.org/10.1063/1.5124387

Appendix

Contributors of this experiment and their affiliations

Suraj Pandey[1], George Calvey[2], Andrea M. Katz[2], Tek Narsingh Malla [1], Faisal H. M. Koua[3], Jose Martin-Garcia[4,6], Ishwor Poudyal[1], Jay-How Yang[4], Mohammad Vakili[5], Oleksandr Yefanov[3], Kara A. Zielinski[2], Saša Bajt[7,8], Salah Awel[3], Katerina Dörner[5], Matthias Frank[9], Luca Gelisio[5], Rebecca Jernigan[4], Henry Kirkwood[5], Marco Kloos[5] ,Jayanath Koliyadu[5], , Valerio Mariani[3], Mitchell D. Miller[10], Grant Mills[5], Garrett Nelson[11], Jose Olmos[10], Alireza Sadri[3], Tokushi Sato[5], Alexandra Tolstikova[3], David Xu[10], Abbas Ourmazd[1], John Spence[11], Peter Schwander[1], Anton Barty[7], Henry N. Chapman[3,8,12], Petra Fromme[4], Adrian P. Mancuso[5,13], George Phillips[10,14], Richard Bean[5], Lois Pollack[2], Marius Schmidt[1].

1. Physics Department, University of Wisconsin-Milwaukee, 3135 N. Maryland Ave,

Milwaukee, Wisconsin 53211, USA

2. School of Applied and Engineering Physics, Cornell University, 254 Clark Hall,

Ithaca, New York 14853, USA

3. Center for Free-Electron Laser Science, Deutsches Elektronen Synchrotron, Notkestrasse 85, 22607 Hamburg, Germany

4. School of Molecular Sciences and Biodesign Center for Applied Structural Discovery, Arizona State University, Tempe, AZ 85287-1604, USA

5. European XFEL GmbH, Holzkoppel 4, 22869 Schenefeld, Germany

6. present address: Institute Physical-Chemistry Rocasolano, Spanish National Research Council, Madrid, Spain

7. Deutsches Elektronen Synchrotron, Notkestrasse 85, 22607 Hamburg, Germany

8. The Hamburg Centre for Ultrafast Imaging, Luruper Chaussee 149, 22761 Hamburg, Germany

9. Lawrence Livermore National Laboratory, 7000 East Avenue, Livermore, CA 94550, USA

10. Department of BioSciences, Rice University, 6100 Main Street, Houston, Texas 77005, USA

11. Department of Physics, Arizona State University, Tempe, Arizona 85287, USA

12. Department of Physics, Universitaet Hamburg, Luruper Chaussee 149, 22761 Hamburg, Germany

13. Department of Chemistry and Physics, La Trobe Institute for Molecular Science, La Trobe University, Melbourne, Victoria 3086, Australia

14. Department of Chemistry, Rice University, 6100 Main Street, Houston, Texas 77005, USA